Physica B: Condensed Matter 570 (2019) 53–57

Contents lists available at ScienceDirect

Physica B: Condensed Matter

journal homepage: www.elsevier.com/locate/physb

Structure and ionic conductivity of new Ga_2S_3-Sb_2S_3-NaI chalcogenide glass system

Yeting Zhang[a], Qing Jiao[a,b,*], Baochen Ma[a], Changgui Lin[a], Xueyun Liu[a,b], Shixun Dai[a,b]

[a] Laboratory of Infrared Material and Devices, Advanced Technology Research Institute, Ningbo University, Ningbo, 315211, China
[b] Key Laboratory of Photoelectric Detection Materials and Devices of Zhejiang Province, Ningbo, 315211, China

ARTICLE INFO

Keywords:
Chalcogenide glasses
Structure
Conductivity
AC impedance method

ABSTRACT

A new glass system of (100-x) ($0.2Ga_2S_3$-$0.8Sb_2S_3$)-xNaI (x = 5–30 mol%) was investigated through a melt-quenching method for solid-state electrolyte application. Na^+ was added into the glass matrix as a conductive ion to study its effect on the properties of glass samples. XRD result indicated that the glasses retained their amorphous state until the NaI content exceeded 30 mol%. With increased NaI component, the density and hardness of glasses slightly decreased. DSC measurement showed that the glass-transition temperature of samples decreased, whereas the glass thermal stability improved. We speculated that the incorporation of NaI may have caused the destruction of [S_3Ga–GaS_3] ethane-like units and formation of [$GaS_{4-x}I_x$] structure, thereby decreasing the connectivity of the glass network. The conductivity of glass samples was further determined using the AC impedance method.

1. Introduction

The depletion of fossil-fuel energy and the aggravation of environmental pollution are becoming increasingly serious, and the identification and development of new sources energy have become particularly important. Traditional cars relying on petroleum energy are now gradually being replaced by new-energy vehicles [1]. Accordingly, research on high-energy batteries, such as sulfur–lithium batteries and sodium–sulfur batteries [2], is receiving widespread attention [3,4]. However, considering the leakage of liquid electrolyte materials, self-ignition, explosion, and other safety issues, solid-state batteries are now a research hotspot [5]. Compared with organic polymers or liquid electrolytes, glass electrolytes can overcome the conventional electrolyte disadvantages [6], such as unstable thermal performance, poor chemical stability, flammability and the need for relatively high operating voltages [7,8]. In addition, the structure of these new materials provides better pathways for fast ion migration aimed at improving battery efficiency in the subsequent solid state energy conversion/storage [9–11].

For example, oxide glass electrolytes are a widely studied type of material with good electrical conductivity. By adding a metal element or a metal halide, the material with good electrical conductivity can be obtained. Interestingly, chalcogenide glasses with higher ionic conductivity is another potential solid-state electrolyte in high-energy-density and good-performance batteries [12,13]. Sulfur ion has a larger radius than oxygen ion, thereby forming a larger ions channel [14,15]. Furthermore, the electronegativity of sulfur ion is smaller than that of oxygen ion, and the binding force to conductive ions is smaller [16,17]. Thus, sulfur ion enables easier conductive-ion transport in a glass network accompanied with a higher battery efficiency [18]. Typically, the ionic conductivity of chalcogenide glass is studied in a sulfur-based glass given its superior mechanical properties compared with selenide glass or telluride glass and its ability to avoid a strong bond energy among atoms [19,20].

In recent reports, a series of chalcogenide-glassy and glass ceramics showed a large room-temperature ionic conductivity of 1.62×10^{-3} S/cm in 40LiI-30Li_2S-27GeS_2-3La_2S_3 glass [21], 1.01×10^{-3} S/cm in 40 ($0.8Sb_2S_3$-$0.2Ga_2S_3$)-60AgI, and 5.4×10^{-3} S/cm in 70Li_2S-29P_2S_5-1P_2S_3 [22]. Furthermore, a novel crystalline-solid electrolyte of $Li_{10}GeP_2S_{12}$ with an ionic conductivity of 1.2×10^{-2} S/cm was prepared successfully [23]. It is the highest ionic conductivity in a solid electrolyte, exceeding even those of liquid organic electrolytes. In the same manner, a high Na^+ conductivity can also be expected in such chalcogenide solid electrolytes. On the basis of the large storage capacity of sodium, easy access, and low cost, the development of all-solid-state rechargeable battery with Na^+ conductors has begun to attract the researchers' attentions. The room-temperature ionic conductivity was 4.6×10^{-4} S/cm in the chalcogenide glass-ceramic electrolyte, when

* Corresponding author. Laboratory of Infrared Material and Devices, Advanced Technology Research Institute, Ningbo University, Ningbo, 315211, China.
E-mail address: jiaoqing@nbu.edu.cn (Q. Jiao).

https://doi.org/10.1016/j.physb.2019.05.026
Received 27 April 2019; Received in revised form 13 May 2019; Accepted 14 May 2019
Available online 17 May 2019
0921-4526/

the cubic Na_3PS_4 phase was precipitated [24]. Although this value is the highest in the currently reported chalcogenide solid electrolyte, it is still several times lower than the oxide solid electrolyte of β-alumina and Nasicon-type $Na_3Zr_2Si_2PO_{12}$ [25]. Na^+-conducting glassy electrolytes with good chemical and thermodynamic stability has been the subject of ongoing research.

In this current work, we reported a new glass of (100-*x*) ($20Ga_2S_3$-$80Sb_2S_3$)-*x*NaI system for the first time. Glasses with NaI content of 30 mol% were manufactured by conventional melt quenching techniques in silica gel ampoules. The effect of NaI addition on glass-structure transition was investigated by X-ray diffraction (XRD), Raman spectra, and Fourier-transform infrared spectroscopy. The ionic conductivity was surveyed by AC impedance spectroscopy.

2. Experimental procedure

The bulk glass having new chemical composition was prepared by melt quenching technique using high purity powder chemicals Ga(5 N), Sb(5 N), S(5 N) and AgI(4 N) under vacuum in a sealed silica tube of 10 and 14 mm as inner and outer diameters, respectively. Then, the silica tube was pumped to the vacuum of approximately 10^{-4} Pa. The sealed tube was heated in a shaker and heated to 850 °C for 12 h. Then, the cooled melts were immediately transferred to a preheated furnace and annealed at a temperature below the glass transition temperature (T_g) of about 30 °C for several hours to minimize internal tension caused by quenching process. The glass sample was sliced and polished to obtain a plate-like sample with a diameter of 10 mm and a thickness of 1.5 mm.

The amorphous nature of the glass was confirmed by XRD measurement using Cu K_α radiation in a power diffractometer (Brook D2, Germany) at 10°–70°. According to the Archimedes principle, the density of the sample was measured using an alcohol as immersion liquid. The microhardness (H_v) was measured using a microhardness tester (Everone MH-3, Everone Enterprises. Ltd., Shanghai, China) at a residence time of 5 s and a test load of 20 gt. Approximately 5 mg of the glass sample of each composition was calorimetrically measured by differential scanning calorimetry (DSC, TA Q2000, USA) at a temperature ranging from 50 to 350 °C. The heating rate was set to 10 °C per minute and purged with N_2 gas. FTIR (Nicolet 380) was used to measure the IR transmission spectra within 2–14 μm. The Raman spectra were collected using a Raman spectrometer (Renishaw In Via, Gloucestershire, UK) by a Ar-ion laser which have an excitation wavelength of 488 nm. The measured excitation power is approximately 2.5 mW. Electrical conductivity was measured using the AC impedance method by Electrochemical Workstation (type: PGSTAT302 N, Metrohm).

3. Results and discussion

In general, T_g of chalcogenide glasses is directly related to several factors, including the glass molar weight, network connectivity, rigidity, and the average energy band [26]. Herein, the DSC trace of samples was obtained at the heating rate of 10 K/min, as presented in Fig. 1. The T_g of glasses ranged from 239 °C to 210 °C with introduction of NaI composition. Traditionally, introducing iodide into the glass destroys the Ga–S bond gradually, thereby forming [GaS_4] units [27]. Glass network connectivity was decreased by iodine atoms that play a non-bridging role. Thus, the NaI addition into the base glass considerably decreased the T_g of the samples. However, the thermal stability of the glass system was well kept, owing to the high difference between T_x and T_g. The higher the value of ΔT, the greater the thermal stability; hence, the easier the glass formation. As shown in Table 1, the ΔT values of all the samples were greater than 120 °C and increased with NaI addition, indicating the improved thermal stability of our samples. For physical properties, the density (ρ) and H_v decreased to some degree when NaI addition increased. Considering the light weight of NaI component, it is easy to understand the evolution of the density.

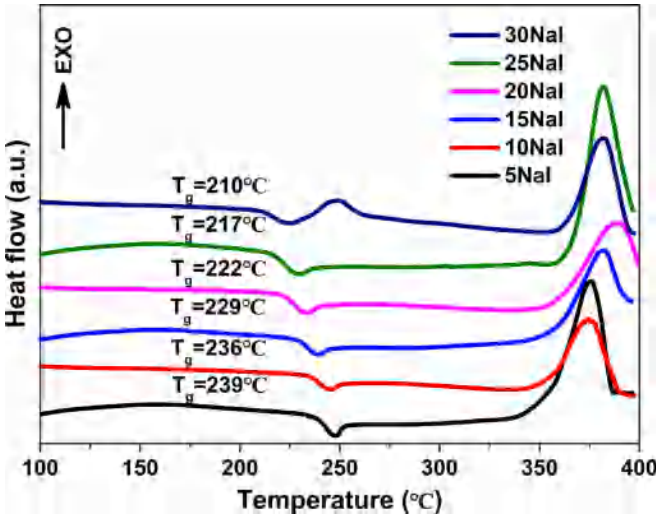

Fig. 1. DSC curves of the glasses with different NaI addition.

Table 1
Thermal and physical properties of Ga_2S_3-Sb_2S_3-*x*NaI glasses.

Compositions	T_g (°C)	T_x (°C)	ΔT (°C)	ρ (g/cm^3)	Hv(kg/mm^2)
x = 5	239	385	146	4.0322	134.41
x = 10	236	389	153	4.0085	123.14
x = 15	229	396	167	3.9924	120.53
x = 20	222	400	178	3.9602	113.02
x = 25	217	397	180	3.9394	106.66
x = 30	210	408	198	3.918	93.78

The addition of an iodine atom which as a glass network terminator to the matrix glass is responsible for the change in glass hardness. The Ga–S bond was destroyed, and the network was then opened broadly, thereby leading to a decrease in hardness.

Considering that these glasses are opaque in the visible spectrum, visual examination is impossible. Hence, XRD was used to determine the amorphous state of glasses. Six diffraction spectrum lines can be seen from Fig. 2, showing a typical amorphous matter halo pattern where no sharp crystallization peak appeared. Thus, no clear crystal phase precipitation occurred, possibly confirming the amorphous state of the glasses. However, the roughness of the XRD curve increased with further addition of iodine atoms, indicating that the sample structure can possibly change from amorphous to crystalline state. Several peaks

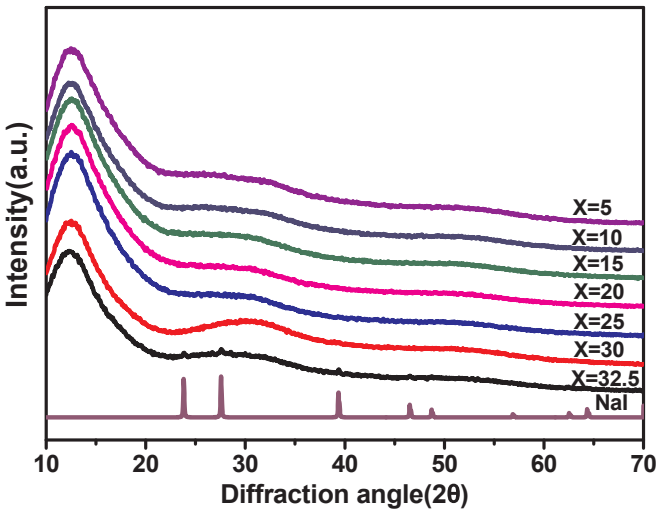

Fig. 2. XRD patterns of all the glasses with reference of standard NaI crystal.

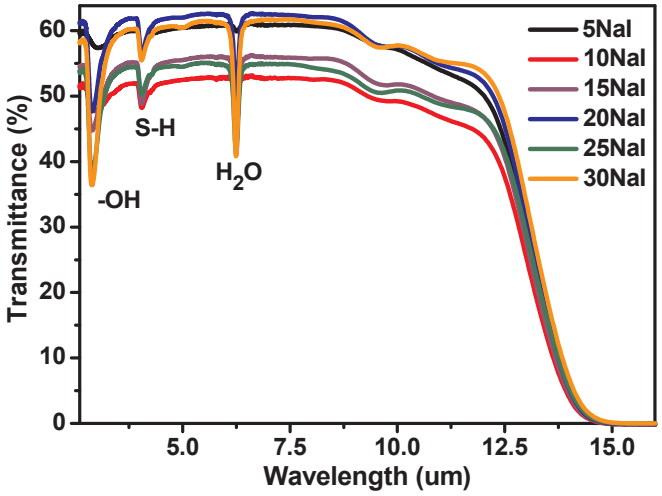

Fig. 3. Infrared transmittance spectra of all the glass samples.

appeared at the following locations: 23.8°, 27.6°, 39.4°, and 46.5°, confirming to the standard NaI crystal (JCPDF card of no.78-602). Such event manifested that the sample began to crystallize when the mole ratio of NaI exceeded 30 mol%. Before the samples were modified by 30 mol% NaI, the glass maintained a good forming ability.

The infrared transmission spectrum of the glass sample measured by Fourier spectrometer is shown in Fig. 3. The cut-off edge of these glasses was at approximately 14 μm, and the IR cut-off edge was mainly affected by the vibration of the Ga–S bond corresponding to the multiphonon process. With NaI addition into the glass, the edges did not clearly change. All of the glass samples exhibited transmittance above 50% which the difference among the maximum transmittance can be due to the heterogeneity of the samples. The vibrational absorption bands were attributed to extrinsic impurities, which belonged to the surface oxidation of the raw materials and the hydroxide contamination during the preparation. Especially, these IR impurity absorption bands were enhanced due to hygroscopicity and increased NaI contents. The absorption bands were situated in 3.0, 3.9, and 6.3 μm in the IR transmittance spectra, assigned to –OH, S–H, and H_2O [28], respectively. If glass prepare by distillation and purification, the impurities can be further diminished as much as possible.

The Nyquist impedance plot of all the glass samples, as shown in Fig. 4, was measured by the AC resistance method. The AC resistance can be calculated from a complex typical Nyquist plot. Zre' and Zim" represent separately the real and imaginary parts of the impedance Z (ω) in the spectrum. The impedance spectra of all samples generally display three different characteristics [29]. The first semicircle of the high frequency corresponds to the ion conducting path in the glass block. The second semicircle indicates the electrode/electrolyte double layer and the resistance of the sample holder and the cable [30]. The third segment follows the low-frequency Warburg impedance of the capacitor-type electrode behavior (linear low peak region) associated with a similar barrier, showing a typical ionic conductor. Theoretically, the total resistance of the bulk electrolyte can be derived from the intersection of arcs with horizontal lines [8]. Glass conductivity may be used $\sigma = L/(SZ_0)$ is calculated, where L is the thickness of the electrolyte, S is the electrolyte - the surface area of the electrode. The intercept of the real part of the impedance map is assigned to Z_0. According to the calculation, the conductivity of the glass sample is on the order of 10^{-10} S/cm, which is relatively lower than that of some reported Na^+ conductive in chalcogenide glasses [17]. In general, the two important keys of conductive ions and ion channels affect the value of ion conductivity in solid-state glass materials. Herein, the chalcogenide solid electrolyte increased in Na^+ conductivity when NaI was added, instead of no apparent regular changes. Moreover, the Ag^+ good electrical conductivity was manifested, but the conductivity of the similar composition of NaI glass was unsatisfactory. Therefore, the reason for the lower conductivity in this experiment may be that the favorable ion channel for Na^+ ions transport was not well formed.

To further understand the reason for the lower conductivity of Na^+ ions, we studied the network structure of representative glass samples with 10, 20, and 30 mol% of NaI by Raman spectra, as shown in Fig. 5. Extensive overlapping peaks at approximately 300 cm^{-1} was assigned to the [SbS_3] pyramid (290 and 314 cm^{-1}). For the [GaS_4] tetrahedral structural unit and the [S_3Ga-GaS_3] ethane-based unit, the shoulder was nearly 138 and 265 cm^{-1} [31,32]. In chalcogenide glass, gallium ions tend to have a four-coordinated coordination with sulfur [33]. Therefore, [S_3Ga-GaS_3] ethane units were formed to compensate for the deficiency of sulfur in the $80Sb_2S_3$-$20Ga_2S_3$ glass. When NaI was added to $80Sb_2S_3$-$20Ga_2S_3$ glass, the Ga–Ga bond in ethane subunit of [S_3Ga-GaS_3] gradually transformed into a [$GaS_{4-x}I_x$] hybrid structure vibrated at 342 cm^{-1} because the Ga–I bond was preferentially formed instead of Ga–S bond [34,35]. Regrettably, the generated [$GaS_{4-x}I_x$] structure units were not beneficial to the transport of the conductive ions. The large I^- ions were substituted for the site of S^{2-} ions, creating the typical [GaS_4]-based tetra-coordinate units. This structure cannot construct the effective transport channels for the conductive Na^+ ions, leading to the relatively lower conductivity.

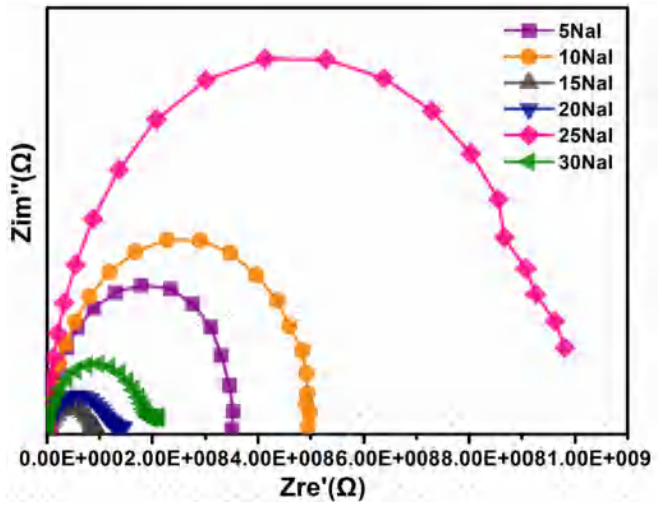

Fig. 4. The Nyquist impedance plots of all the glass samples at room temperature.

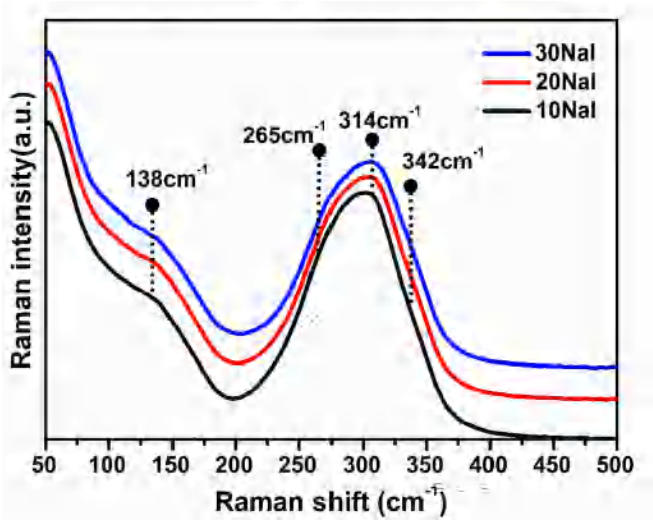

Fig. 5. Raman spectra of samples with addition of 10, 20 and 30 mol% NaI.

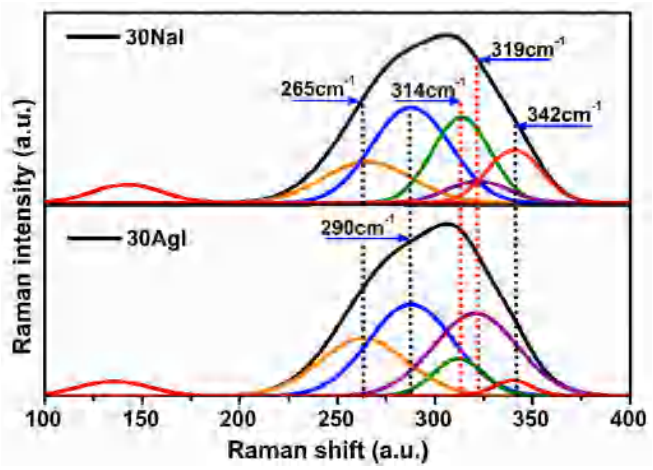

Fig. 6. Raman spectra of Ga-Sb-S glasses doped with same amount of AgI and NaI.

Comparison of the Raman spectra in 30 mol% NaI and 30 mol% AgI modified same glass matrix are presented in Fig. 6. The detailed peak-differentiating and imitating results are listed to better understand the structural changes in NaI-based sample. Clearly, the area ranging from 200 cm^{-1}–400 cm^{-1} included five Raman bands located at 265, 290, 314, 319, and 342 cm^{-1}. For the $Ga_2S_3-Sb_2S_3-NaI$ glasses, three Raman peaks centered at 290, 314, and 319 cm^{-1} can be resolved by those of $[SbS_3]$ and $[SbS_{3-x}I_x]$ units [36,37]. Furthermore, the other peaks centered at 265 and 342 cm^{-1} can be explained by $[S_3Ga\text{-}GaS_3]$ ethane units and $[GaS_{4-x}I_x]$ hybrids. Compared with those of AgI glass, the peaks at 265 and 319 cm^{-1} of NaI sample decreased significantly, and the peaks at 314 and 342 cm^{-1} improved apparently. Therefore, the networks of the $Ga_2S_3-Sb_2S_3-NaI$ glasses were constructed mainly from $[GaS_{4-x}I_x]$ tetrahedral, which cannot build an effective transport channel for movable ions. Conversely, the main AgI glass structure was $[SbS_{3-x}I_x]$ units, which are considerably beneficial for ion conductivity [38]. Thus, the NaI samples had a relatively lower ionic conductivity than AgI-based conductive glass. Herein, iodine ions may preferentially form a covalent bond with the Ga atom, and the Na^+ ion or the Ag^+ ion was freed in the glass network structure after AgI or NaI was added in the glass. Owing to the higher electronegativity of Ag^+ (1.93) than Na^+ (0.93), it may attract the iodine element in $[GaS_{4-x}I_x]$ units and form the $[SbS_{3-x}I_x]$ structure with the Sb element. In addition, the electronegativity of Na ion was smaller than Ga (1.81), indicating an insufficient strength to attract iodine atom in $[GaS_{4-x}I_x]$ units. Therefore, NaI was added to the matrix glass to preferably form $[GaS_{4-x}I_x]$ units, whereas the added AgI tended to form $[SbS_{3-x}I_x]$ units, creating the effective ion-travelling channel contributing for a high conductivity.

4. Conclusions

The glass of the Ga_2S_3-Sb_2S_3-NaI system was successfully prepared, and the effects of the addition of NaI on the thermal, optical, electrical conductivity and structural properties of these glasses were determined. Good glass-forming ability was identified until 30 mol% of dopant sample was attained by XRD, and then few NaI crystals began to precipitate from the matrix. The density and hardness of the glasses decreased reasonably with increase of NaI modification, yet the thermal ability was greatly enhanced according to the DSC analysis. Combined with the result of Raman spectroscopy, the incorporation of iodine ions resulted in the destruction of $[S_3Ga\text{-}GaS_3]$ ethane units and formed the tetrahedral $[GaS_{4-x}I_x]$ structure, thereby reducing the connectivity of the glass network and the glass transition temperature of the glass. In addition, the influence of NaI on the ionic conduction behavior was also investigated for all the samples. Unlike that in the AgI-modified chalcogenide glass, the lower conductivity of NaI samples totally exceeded the prediction. Thus, an effective ion transport channel may be attacked by the conductive ions, thereby impairing the higher conductivity ability. Therefore, not only the conductive ions and transport channel but also the relationship between them should be further considered to enhance the ionic conductivity in this chalcogenide system.

Acknowledgement

This work was supported by Natural National Science Foundation of China (NSFC) (Grant no. 61605093 and 51702172), Natural Science Foundation of Ningbo City (No. 2018A610140), National Key Research and Development Program of China (No. 2016YFB0303803 and 2016YFB0303802) and sponsored by K. C. Wong Magna Fund in Ningbo University.

References

[1] L. Zhanqiang, T. Yufeng, L. Xujie, R. Guohao, H. Fuqiang, Enhanced ionic conductivity of sulfide-based solid electrolyte by incorporating lanthanum sulfide, Ceram. Int. 40 (10) (2014) 15497–15501.
[2] V. Etacheri, R. Marom, R. Elazari, G. Salitra, D. Aurbach, Challenges in the development of advanced Li-ion batteries: a review, Energy Environ. Sci. 4 (9) (2011) 3243–3262.
[3] M. Armand, J.M. Tarascon, Building better batteries, Nature 451 (7179) (2008) 652–657.
[4] R. Seshadri, K. Persson, P.V. Kamat, W. Yiying, Recent advances in battery science and technology, Chem. Mater. 27 (13) (2015) 4505–4506.
[5] W. Ning, Y. Kun, Z. Long, Y. Xinlin, W. Limin, X. Bo, Improvement in ion transport in Na3PSe4-Na3SbSe4 by Sb substitution, J. Mater. Sci. 53 (3) (2018) 1987–1994.
[6] N. Tanibata, K. Noi, A. Hayashi, M. Tatsumisago, Preparation and characterization of Na3PS4-Na4GeS4 glass and glass-ceramic electrolytes, Solid State Ionics 320 (2018) 193–198.
[7] J.E. Trevey, Y.S. Jung, S.H. Lee, High lithium ion conducting LiS-GeS-PS glass-ceramic solid electrolyte with sulfur additive for all solid-state lithium secondary batteries, Electrochim. Acta 56 (11) (2011) 4243–4247.
[8] Z. Long, Y. Kun, M. Jianli, Z. Linran, W. Limin, L. Yueming, Z. Hong, Na3PSe4: a novel chalcogenide solid electrolyte with high ionic conductivity, Adv. Energy Mater. 5 (24) (2016) 39–41.
[9] S. Song, H.M. Duong, A.M. Korsunsky, N. Hu, L. Lu, A Na+ superionic conductor for room-temperature sodium batteries, Sci. Rep. 6 (2016) 32330.
[10] T. Minami, A. Hayashi, M. Tatsumisago, Recent progress of glass and glass-ceramics as solid electrolytes for lithium secondary batteries, Solid State Ionics 177 (26) (2006) 2715–2720.
[11] Z. Jianhua, L. Lei, Y. Haiwei, W. Yang, W. Jie, C. Guorong, Effects of the Se substitution for Te on the structure and properties of glasses in the Ag30As28(SexTe100-x)42 system, Ceram. Int. 45 (7, Part A) (2019) 9136–9139.
[12] R.W. Haisty, H. Krebs, Electrical conductivity of melts and their ability to form glasses: I. The Ge-Sb-Se system, J. Non-Cryst. Solids 1 (5) (1969) 399–426.
[13] D. Fasquelle, J.C. Carru, C. Renard, Electrical characterizations of silver chalcogenide glasses, J. Non-Cryst. Solids 353 (11–12) (2007) 1120–1125.
[14] Y. Kawamoto, S. Tsuchihashi, Properties and structure of glasses in the system Ge-S, J. Am. Ceram. Soc. 54 (3) (1971) 131–135.
[15] K. Minami, A. Hayashi, M. Tatsumisago, Crystallization process for superionic Li7P3S11 glass-ceramic electrolytes, J. Am. Ceram. Soc. 94 (6) (2011) 1779–1783.
[16] J. Saienga, Y. Kim, B. Campbell, S. Martin, Preparation and characterization of glasses in the LiI + Li2S + GeS2 + Ga2S3 system, Solid State Ionics 176 (13) (2005) 1229–1236.
[17] W. Yao, S.W. Martin, Ionic conductivity of glasses in the MI + M2S + (0.1Ga2S3 + 0.9GeS2) system (M = Li, Na, K and Cs), Solid State Ionics 178 (33) (2008) 1777–1784.
[18] H.K. Patel, S.W. Martin, Fast ionic conduction in Na2S + B2S3 glasses, Compositional contributions to nonexponentiality in conductivity relaxation in the extreme low-alkali-metal limit, Phys. Rev. B 45 (18) (1992) 10292–10300.
[19] A. Hayashi, K. Minami, M. Tatsumisago, Development of sulfide glass-ceramic electrolytes for all-solid-state lithium rechargeable batteries, J. Solid State Electrochem. (10) (2010) 1761–1767.
[20] F. Bo, F. Huang, L. Haiyang, X. Bai, Z. Xianghua, L. Zhongkuan, M. Hongli, Ionic conductive GeS2-Ga2S3-Li2S-LiI glass powders prepared by mechanical synthesis, J. Alloy. Comp. 740 (2018) 61–67.
[21] J. Saienga, S.W. Martin, The comparative structure, properties, and ionic conductivity of LiI + Li2S + GeS2 glasses doped with Ga2S3 and La2S3, J. Non-Cryst. Solids 354 (14) (2008) 1475–1486.
[22] A. Hayashi, K. Minami, S. Ujiie, M. Tatsumisago, Preparation and ionic conductivity of Li7P3S11-z glass-ceramic electrolytes, J. Non-Cryst. Solids 356 (44) (2010) 2670–2673.
[23] N. Kamaya, K. Homma, Y. Yamakawa, M. Hirayama, R. Kanno, M. Yonemura, T. Kamiyama, Y. Kato, S. Hama, K. Kawamoto, A. Mitsui, A lithium superionic conductor, Nat. Mater. 10 (9) (2011) 682–686.

[24] A. Hayashi, K. Noi, N. Tanibata, M. Nagao, M. Tatsumisago, High sodium ion conductivity of glass-ceramic electrolytes with cubic Na3PS4, J. Power Sources 258 (2014) 420–423.
[25] H. Khireddine, P. Fabry, A. Caneiro, B. Bochuc, Optimization of nasicon composition for Na+ recognition, Sensor. Actuator. B Chem. 40 (2–3) (1997) 223–230.
[26] L. Calvez, M. Hongli, J. Lucas, Z. Xianghua, Selenium-based glasses and glass ceramics transmitting light from the visible to the Far-IR, Adv. Mater. 38 (12) (2010) 129–132.
[27] Z. Li, L. Changgui, Q. Guoshun, L. Calvez, D. Shixun, Z. Xianghua, X. Tiefeng, N. Qiuhua, Formation and properties of chalcogenide glasses based on GeS2-Sb2S3-AgI system, Mater. Lett. 132 (10) (2014) 203–205.
[28] M. Zhang, Y. Anping, P. Yunfeng, Z. Bin, R. He, G. Wei, Y. Yan, Z. Chengcheng, W. Yuwei, Y. Zhiyong, T. Dingyuan, Dy3+-doped Ga-Sb-S chalcogenide glasses for mid-infrared lasers, Mater. Res. Bull. 70 (2015) 55–59.
[29] W. Junjun, K. Hyea, L. Dongchan, H. Renzhong, Influence of annealing on ionic transfer and storage stability of Li2S-P2S5 solid electrolyte, J. Power Sources 294 (2015) 494–500.
[30] S.K. Kim, A. Mao, S. Sen, S. Kim, Fast Na-ion conduction in a chalcogenide glass-ceramic in the ternary system Na2Se-Ga2Se3-GeSe2, Chem. Mater. 26 (19) (2014) 5695–5699.
[31] R. Jing, Y. Qiqi, W. Tomas, Z. Vitezslav, F. Miloslav, F. Bozena, C. Guorong, Conductivity study on GeS2-Ga2S3-AgI-Ag chalcohalide glasses, J. Appl. Phys. 114 (2) (2013) 1070–1073.
[32] Y. Anping, Q. Jiahua, Z. Mingjie, S. Mingyang, Y. Zhiyong, Mid-infrared luminescence of Dy3+-doped Ga2S3-Sb2S3-CsI chalcohalide glasses, Chin. Phys. B 27 (7) (2018) 077105.
[33] A. Anderson, S.K. Sharma, S.Y. Wang, Z. Wang, Raman study of antimony triiodide at high pressures, J. Raman Spectrosc. 29 (4) (1998) 251–255.
[34] Y. Anping, Z. Mingjie, L. Lei, W. Yuwei, Ga-Sb-S chalcogenide glasses for mid-infrared applications, J. Am. Ceram. Soc. 99 (1) (2016) 12–15.
[35] Z. Mingjie, Y. Zhiyong, Z. Hua, Y. Anping, L. Lei, T. Haizheng, Glass forming and properties of Ga2S3-Sb2S3-CsCl chalcohalide system, J. Alloy. Comp. 722 (2017) 166–172.
[36] M. Tamilselvan, A.J. Bhattacharyya, Antimony sulphoiodide (SbSI), a narrow band-gap non-oxide ternary semiconductor with efficient photocatalytic activity, RSC Adv. 6 (107) (2016) 105980–105987.
[37] G. HaiTao, Z. MingJie, X. YanTao, X. XuSheng, Y. ZhiYong, Structural evolution study of additions of Sb2S3 and CdS into GeS2 chalcogenide glass by Raman spectroscopy, Chin. Phys. B 26 (10) (2017) 104208.
[38] L. Changgui, Z. Erwei, W. Jingson, Z. Xuhao, Fast Ag-ion conducting GeS2-Sb2S3-AgI glassy electrolytes with exceptionally low activation energy, J. Phys. Chem. C 122 (3) (2018) 1486–1491.